Anal. Chem. **2006,** *78,* 7751−7760

Characterizing Electrospray Ionization Using Atmospheric Pressure Ion Mobility Spectrometry

Xiaoting Tang, James E. Bruce, and Herbert H. Hill, Jr.*

Department of Chemistry, Washington State University, Pullman, Washington 99164

Reduced flow rate electrospray ionization has been proven to provide improved sensitivity, less background noise, and improved limits of detections for ESI-MS analysis. Miniaturizing the ESI source from conventional electrospray to microelectrospray and further down to nanoelectrospray has resulted in higher and higher sensitivity; however, when effects of flow rate were investigated for atmospheric pressure ESI-IMS using a nanospray emitter, a striking opposite result was observed. The general tendency we observed in ESI-IMS was that higher flow rate offered higher ion signal intensity throughout a variety of conditions investigated. Thus, further efforts were undertaken to rationalize these contradictory results. It is well accepted that decreased flow rate increases both ionization efficiency and transmission efficiency, thus improving ion signal in ESI-MS. However, our study revealed that decreased flow rate results in decreased ion signal because ion transfer is constant, no matter how flow rate changes in ESI-IMS. Since ion transfer is constant in atmospheric pressure ESI-IMS, ionization efficiency can be studied independently, which otherwise is not possible in ESI-MS in which both ionization efficiency and transmission efficiency vary as conditions alter. In this article, we present a systematic study of signal intensity and ionization efficiency at various experimental conditions using ESI-IMS and demonstrate the ionization efficiency as a function of flow rate, analyte concentration, and solvent composition.

Electrospray ionization (ESI), an atmospheric ionization technique used to generate gas-phase ions by spraying analyte solution at high voltage, was first introduced by Dole et al. in 1968.[1] Fenn et al. further demonstrated the applications of ESI in mass spectrometry (MS) techniques in the early 1980s[2,3] and received the Nobel prize in chemistry in 2002 due to this invention. ESI has become one of the most important and powerful ionization techniques for MS because of its effectiveness in detecting large biomolecules[4] and ease-of-use for interfacing liquid-based separation techniques, such as liquid chromatography (LC)[5,6] and capillary electrophoresis.[7−9]

A conventional ESI source typically employs flow rates in the range of 4−200 μL/min through a capillary that has 50−200-μm inner diameter (i.d.).[5] A microelectrospray source makes use of a tapered emitter with a small terminal orifice (usually <20-μm i.d.) and much lower flow rates in the range of 0.1−1 μL/min. The use of a low flow rate in ESI-MS has proven advantageous in detection of biological molecules, since it shows significantly improved sensitivity.[10,11] At nanoliter-per-minute flow rates, the attomole limit of detection of proteins is possible.[12] With these successes, the edge of the envelope was further pushed by Wilm and Mann,[13,14] who introduced nanoelectrospray (or nanospray) ionization with further decreased flow rate. Without the use of a solvent pump, this static nanospray ion source allows the liquid to flow through the spray emitter by capillary action when a high voltage is applied. The measured flow rate is as low as 20−40 nL/min through a very small tip that has ~1-μm i.d. It is believed that the lower flow rate provides better ionization efficiency because it produces smaller initial charged droplets that require less solvent evaporation and fewer droplet fission events prior to eventual ion release in the gas phase.[15,16] In addition, the closer alignment at the interface between the emitter tip and the MS inlet aperture or capillary and the elimination of the need for sheath flow and sheath gas with the use of nanospray source have been proven to improve ion transmission efficiency.[17] As a result,

* To whom correspondence should be addressed. E-mail: hhhill@wsu.edu.

(1) Dole, M.; Mach, L. L.; Hines, R. L.; Mobley, R. C.; Ferguson, L. P.; Alice, M. B. *J. Chem. Phys.* **1968**, *49*, 2240−2249.
(2) Yamashita, M.; Fenn, J. B. *J. Phys. Chem.* **1984**, *88*, 4451−4459.
(3) Yamashita, M.; Fenn, J. B. *J. Chem. Phys.* **1984**, *88*, 4671−4675.
(4) Fenn, J. B.; Mann, M.; Meng, C. K.; Wong, S. F.; Whitehouse, C. M. *Science* **1989**, *246*, 64−71.
(5) Whitehouse, C. M.; Dreyer, R. N.; Yamashita, M.; Fenn, J. B. *Anal. Chem.* **1985**, *57*, 675−679.
(6) Bruins, A. P.; Covey, T. R.; Henion, J. D. *Anal. Chem.* **1987**, *59*, 2642−2646.
(7) Smith, R. D.; Loo, J. A.; Edmonds, C. G.; Barinaga, C. J.; Udseth, H. R. *J. Chromatogr.* **1990**, *516*, 157−165.
(8) Hofstadler, S. A.; Swanek, F. D.; Gale, D. C.; Ewing, A. G.; Smith, R. D. *Anal. Chem.* **1995**, *67*, 1477−1480.
(9) Lee, E. D.; Mueck, W.; Henion, J. D.; Covey, T. R. *Biomed. Environ. Mass Spectrom.* **1989**, *18*, 844−850.
(10) Gale, D. C.; Smith, R. D. *Rapid Commun. Mass Spectrom.* **1993**, *7*, 1017−1021.
(11) Andren, P. E.; Emmett, M. R.; Caprioli, R. M. *J. Am. Soc. Mass Spectrom.* **1994**, *5*, 867−869.
(12) Valaskovic, G. A.; Kelleher, N. L.; McLafferty, F. W. *Science* **1996**, *273*, 1199−1202.
(13) Wilm, M.; Mann, M. *Int. J. Mass Spectrom. Ion Processes* **1994**, *136*, 167−180.
(14) Wilm, M.; Mann, M. *Anal. Chem.* **1996**, *68*, 1−8.
(15) Juraschek, R.; Dulcks, T.; Karas, M. *J. Am. Soc. Mass Spectrom.* **1999**, *10*, 300−308.
(16) Schmidt, A.; Karas, M.; Dulcks, T. *J. Am. Soc. Mass Spectrom.* **2003**, *14*, 492−500.
(17) Smith, R. D.; Shen, Y.; Tang, K. *Acc. Chem. Res.* **2004**, *37*, 269−278.

10.1021/ac0613380 CCC: $33.50
Published on Web 10/17/2006

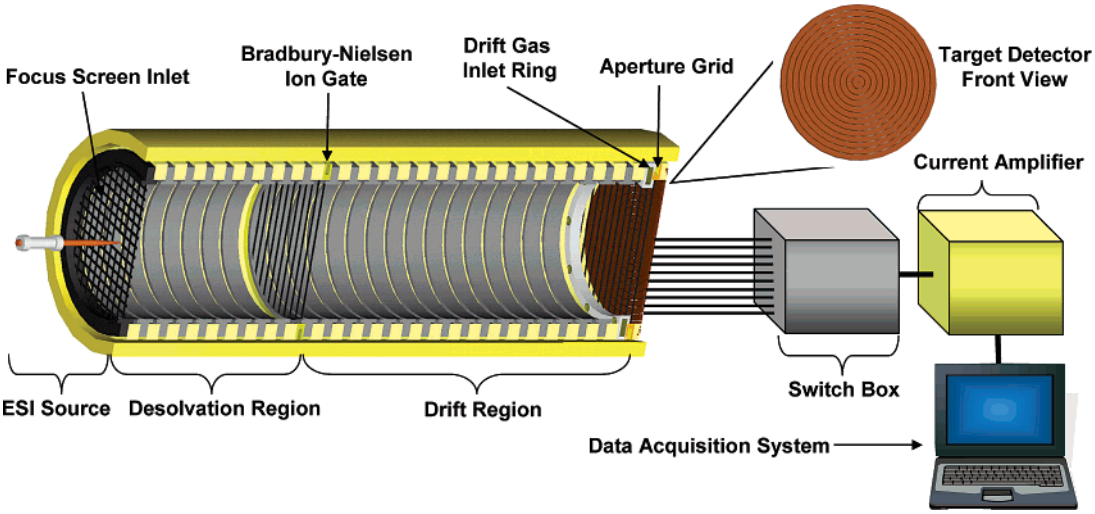

Figure 1. Schematic of the atmospheric pressure ESI-IMS instrument with target Faraday collector.

the overall detection efficiency, hence sensitivity, is significantly enhanced.

A few years after the development of ESI, Dole and co-workers demonstrated the detection of lysozyme with unresolved charge states by coupling ESI for ion mobility spectrometry (IMS).[18] Similar ESI-IMS spectra of lysozyme and cytochrome *c* were reported by Smith and co-workers in 1991.[19] We further advanced ESI-IMS in the analysis of large molecules with improved sensitivity and resolution by incorporating a counter flow heated drift gas[20−21] and a water-cooled ESI source.[22] Very recently, Creaser and co-workers reported the first application of nanoESI in an atmospheric pressure ion mobility spectrometer.[23,24] However, unlike nanoESI-MS, which shows great sensitivity with use of low micromolar to nanomolar concentrations of the analyte solution, in their studies, instead, significantly higher concentrations of solution (>5 mM) were required to obtain signals for peptides in ESI-IMS. No systematic study of various flow rates ranging from nanoliters to microliters per min for ESI-IMS has been reported yet.

To this end, we have looked into the rationale behind the opposite flow rate effects observed in ESI-IMS. We designed and implemented a target Faraday detector to characterize ion transmission in ESI-IMS. With constant ion transmission and minimal loss through the drift space, we were able to characterize electrospray ionization efficiency under various experimental parameters. In this report, the unique atmospheric pressure ion detection property offered by IMS was utilized for the first time to evaluate and compare ionization efficiency for an electrospray ion source.

(18) Gieniec, M. L.; Cox, J., Jr.; Teer, D.; Dole, M. Dallas, TX, June 4−9, 1972.
(19) Smith, R. D.; Loo, J. A.; Ogorzalek, R. R.; Busman, M.; Udseth, H. R. *Mass Spectrom. Rev.* **1991**, *10*, 359−452.
(20) Shumate, C. B.; Hill, H. H. Bellingham, WA, June 1987.
(21) Shumate, C. B.; Hill, H. H. *Anal. Chem.* **1989**, *61*, 601−606.
(22) Wittmer, D.; Chen, Y. H.; Luckenbill, B. K.; Hill, H. H. *Anal. Chem.* **1994**, *66*, 2348−2355.
(23) Bramwell, C. J.; Colgrave, M. L.; Creaser, C. S.; Dennis, R. *Analyst* **2002**, *127*, 1467−1470.
(24) Colgrave, M. L.; Bramwell, C. J.; Creaser, C. S. *Int. J. Mass Spectrom.* **2003**, *229*, 209−216.

EXPERIMENTAL SECTION

Chemicals and Reagents. Methanol (MeOH) used in this study was HPLC grade and obtained from J. T. Baker (Phillipsburgh, NJ). Acetic acid (HOAc) and hydrofluoric acid (HF) were obtained from Sigma (St. Louis, MO). Water was 18-MΩ deionized, prepared by Barnstead Nanopure Water Systems. Cocaine, amphetamine, and caffeine were purchased from RBI (Natick, MA). L-Serine was purchased from Sigma (St. Louis, MO).

Ion Mobility Spectrometer. The atmospheric pressure ion mobility spectrometer used for this research was constructed at Washington State University, Pullman, WA. The instrument configuration is shown in Figure 1. The drift tube was built upon a standard stacked ring configuration by assembling repeating units. Each repeating unit, composed of a conductive stainless steel ring with dimensions of 50 mm (o.d.) × 48 mm (i.d.) × 3 mm (width) and an insulating ceramic ring with dimensions of 60 mm (o.d.) × 50 mm (i.d.) × 4.5 mm (width), is stacked sequentially in an alumina tube. The stainless steel rings, also called guard rings, were connected via a series of 0.5- (desolvation region) and 1-MΩ (drift region) resistors (Caddock Electronics Inc., Riverside, CA). The ceramic ring served to isolate the guard rings from the alumina tube as well as from each other. The current instrument consists of 42 repeating units with a total length of 34 cm, but the length of the drift tube can be easily shortened or lengthened by removing or adding a number of rings. A Bradbury−Nielsen gate ring divided the drift tube into a 7.5-cm-long desolvation region and a 26.5-cm-long drift region. A 10-kV voltage was normally applied to the first ring electrode, and the last ring electrode voltage was adjusted by a variable resistor to be ~200 V referenced to ground. The drift voltage was dropped gradually across the drift tube via the resistor chain to form an electric field of 157 V/cm in the desolvation region and 333 V/cm in the drift region. The lower electric field in the desolvation region allowed solvated ions to spend more time in the heated drift gas to get more efficient desolvation prior to injection to the drift region. The Bradbury−Nielsen gate was made of electrically isolated alternating parallel alloy 46 wires (76 μm in diameter) (California Fine Wire Co., Grover Beach, CA) spaced 0.65 mm apart. When the potentials applied on the alternating wires were

the same as the reference potential, the gate was "open" to allow ions to pass through, whereas the potentials on the adjacent wires were offset ±50 V with respect to the reference potential, an electric field of ~1500 V/cm was created orthogonal to the drift field, and the gate was "closed" to shut off ion transmission.

An aperture grid ring, made in a manner similar to that of the Bradbury−Nielsen gate ring with the exception that adjacent wires were in common, was placed right in front of the terminal Faraday plate (60 mm in diameter) with ~0.5 mm spacing. The function of the aperture grid was to shield the incoming ion cloud from the detector prior to its arrival and reduce peak broadening. The counter flow drift gas was introduced to the drift tube near the tube terminus through a hollow drift ring that had eight radially distributed apertures. The drift tube oven was constructed from two pieces of 20-cm-long aluminum cylinder with three heating cartridges (Heatcon, Seattle, WA) embedded inside each cylinder. The electronics system used for the instrument included a high-voltage power supply for the ESI emitter, a high-voltage power supply for the drift tube, a two-channel temperature controller for the drift tube oven, a gate controller, and a current amplifier for signal amplification. The data acquisition software was programmed in LabVIEW 6.1 (National Instruments, Austin, TX) and communicated with the gate controller and current amplifier through an interface board (PCI-6030E) (National Instruments, Austin, TX) installed in a Dell PC computer.

Target Faraday Detector. To investigate the ion beam's distribution at the drift tube exit, we designed and built a targetlike, segmented, Faraday plate detector (Figure 1), which was composed of a set of concentric copper rings mounted on an insulating support. Each copper ring, measured ~2 mm wide and separated from the adjacent rings by a space of ~0.2 mm, was attached to an individual lead that was wired to the current amplifier separately through a switch box. The diameter of each ring increased radially because it was further away from the center; for example, ring 1 in the center has an o.d. of 5 mm, and ring 12 at the edge has an o.d. of 49 mm. The ion signal can be either measured individually for each ring or measured with any combined number of rings with all other rings grounded. The charge density (C/mm^2) was calculated by dividing the peak area by the surface area of the respective ring.

NanoESI Source. The nanospray emitter was made by etching a fused-silica capillary (360-μm o.d. × 20-μm i.d., Polymicro Technologies, Phoenix, AZ) in 49% HF solution. The wall thickness of the emitter terminus was thinned down to ≤0.1 μm after 30 min to 1 h of etching. The emitter was then cut to be ~5 cm long. The relatively large tip aperture (20-μm i.d.) was chosen for this research because it allowed the liquid to be delivered through the emitter at a relatively wide range of flow rates. Normally, the flow rate was varied from 0.1 to 10 μL/min using the solution delivered from the same syringe (250-μL Hamilton gastight syringe, Reno, NV) for the entire set of the experiments, which ensured consistency throughout. Flow rates over 12 μL/min often caused backpressure over time and eventually broke weak connections between the syringe needle and the injection port. The electrical contact was applied through a stainless steel zero-dead-volume union (Upchurch Scientific, Oak Harbor, WA) that connected the emitter with the fused-silica capillary transfer line (360-μm o.d. × 75-μm i.d., ~30 cm long).

Operating Conditions. Electrospray ionization was normally induced by applying a potential difference of 2.5−3.5 kV between the nanospray emitter and the target focus screen (16-mesh stainless steel), which also served as the first ring electrode for the drift tube. A hole with ~5-mm diameter was punched in the center of a 16-mesh screen inlet. The optimal signal was usually observed when the nanospray emitter was positioned in the center of the hole with the tip terminus inserted through the mesh screen for 3−5 mm. A voltage of 10 kV was typically applied to the first ring electrode, and 12.5−13.5 kV was used for the nanospray emitter. It should be noted that the effective drift voltage across the drift region was the potential difference between the gate ring and the aperture grid ring (typically ~8.6 kV) but not total applied voltage. The drift tube was normally heated at 200−250 °C. N_2 was used as the counter flow drift gas throughout the experiments and was injected into the drift tube at a constant flow rate of 500 mL/min to sweep out neutral interferences during spectral acquisitions.

All experiments were carried out at atmospheric pressure, which typically ranged from 690 to 710 Torr in Pullman, WA. The solvent used for most experiments was a mixture of 50% MeOH/45% H_2O/5% HOAc unless otherwise specified. A syringe pump (KD Scientific, Holliston, MA) was used to deliver solution to the spray emitter at the desired flow rate. The charged droplets emitting from ionization source were further desolvated by heated drift gas while migrating slowly in the desolvation region, and desolvated ions were then injected into the drift region by opening the ion gate for a brief 0.2-ms pulse width at a frequency of 20 Hz. The target Faraday detector was used only to acquire spectra for the charge and current distribution study. All the other experiments used the regular Faraday plate. The current amplifier gain was usually set at 10^9 V/amp. Each IMS spectrum was data-averaged from 500 gate pulses. Three to five IMS spectra were acquired consecutively to obtain one averaged data point (peak intensity).

Safety Considerations. Since high voltages were used in the ESI source and IMS, only trained personnel was allowed to operate the instruments, and warning signs were posted to keep the site clear when the instrument was in operating mode.

RESULTS AND DISCUSSION

It is well accepted that the sensitivity of ESI-MS measurements improves inversely with liquid flow rate. Miniaturizing the ionization source from conventional ESI to nano ESI has resulted in signal improvements by orders of magnitude. Nanospray ionization using small tip diameters of a few micrometers and a low flow rate in nanoliters per minute has been the method of choice in most biological mass spectrometry laboratories because of limited sample quantity. However, when nanospray was applied to a stand-alone atmospheric pressure IMS instrument, an opposite flow rate effect was observed; i.e., the ion signal intensity steadily increased with the increased flow rate. Thus, further experiments were carried out in this study to look into the rationale behind these contradictory observations.

Initial Observations of Flow Rate Effects. A nanospray emitter that was normally used for nanoESI-MS applications in

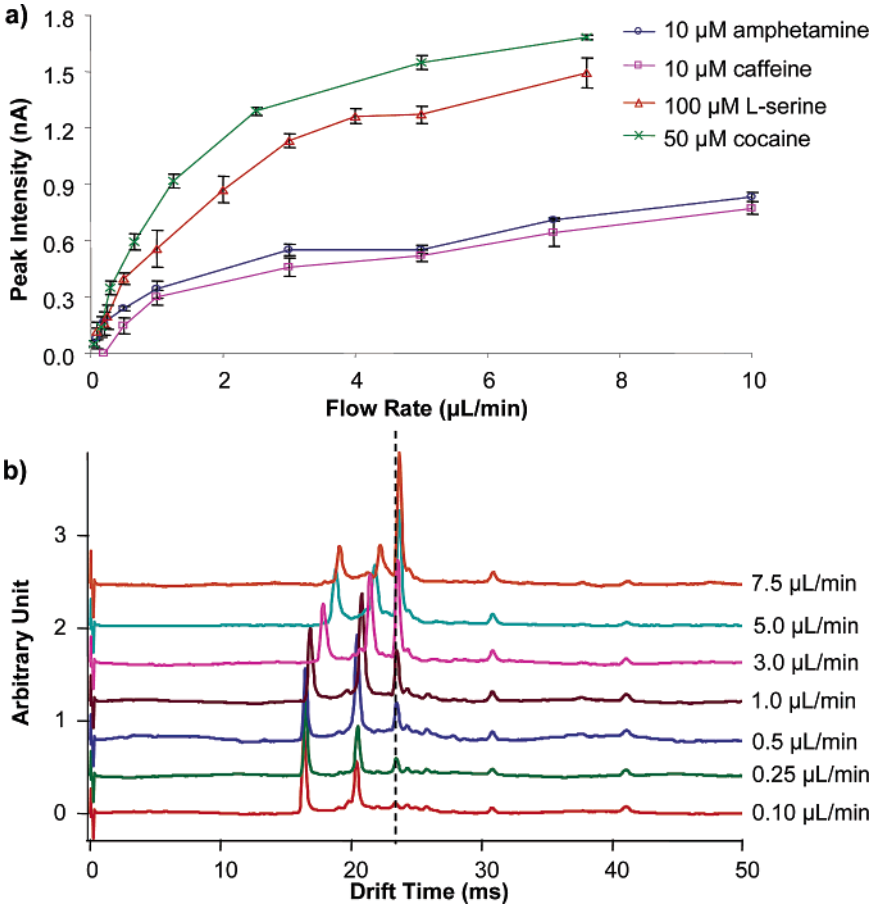

Figure 2. Observation of increased ion signal response with increased flow rate in ESI-IMS. (a) Plots of ion signal intensity as a function of flow rate for four different compounds, 10 μM amphetamine, 10 μM caffeine, 100 μM L-serine, and 50 μM cocaine. (b) Overlay of 7 IMS spectra of 100 μM serine at various flow rates.

our laboratory[25,26] was employed for all the ESI-IMS experiments in this study. The spray emitter was made by etching a fused-silica capillary (360-μm o.d. × 20-μm i.d.) with HF solution until a thin wall (50−80-nm thickness)[10,27] was formed at the tip's terminus. The extremely thin terminal wall thickness helps generate a high electric field for stable electrospray.[28] Initially, it was expected that better sensitivity should be achieved with nanospray than with microspray (50-μm tip i.d., 2−5 μL/min flow rate) that was routinely used for ESI-IMS in our lab.[29,30] However, ion signals proportionally increased with increased flow rates when 100 ppb lutidine samples were electrosprayed into the IMS. Thus, further investigations were conducted by using a variety of compounds at different concentrations. Consistent results were observed throughout all the experiments.

Figure 2 shows a few selected examples, including 50 μM cocaine, 100 μM L-serine, 10 μM amphetamine, and 10 μM caffeine. Note that each set of data for these four compounds was acquired in different times under different experimental conditions, such as different spray tips and voltages. However, in all cases, the ion signals increased with increased flow rates. These observations seemed to indicate that the ESI-IMS response is mass-sensitive rather than concentration-sensitive, which is exactly opposite to the common findings in ESI-MS. Figure 2b shows the full ESI-IMS spectra of 100 μM L-serine with flow rates ranging from 0.1 to 7.5 μL/min. As shown in the figure, the peak intensity for L-serine with a drift time of ~23.5 ms increased steadily with flow rate. However, signal intensities for the two solvent ion peaks exhibited the opposite trend; i.e., a higher response was obtained at a lower flow rate. In addition, their drift times shifted dramatically to longer times (the first solvent peak went from a drift time of 16.4−19.1 ms, and the second solvent peak migrated from 20.4 to 22.2 ms when the flow rate changed from 0.1 to 7.5 μL/min). These observations for the solvent peaks indicated that at higher flow rate, larger solvent cluster ions were created, and the solvent components (H_2O, MeOH, and HOAc) were ionized less sufficiently, which conformed to the results one would expect from an ESI-MS experiment. Furthermore, it was found that the drift time of L-serine was slightly shifted to a longer time as the flow rate increased, from 23.4 ms at 0.1 μL/min to 23.6 ms at 7.5 μL/min. Hill et al. reported previously that the reduced mobility values for some analytes by using ESI-IMS are lower than those by ^{63}Ni-IMS and suggested this is the consequence of incomplete

(25) Wu, S.; Tang, X. T.; Siems, W. F.; Bruce, J. E. *J. Chromatogr., B* **2005**, *822*, 98−111.
(26) Tang, X.; Munske, G. R.; Siems, W. F.; Bruce, J. E. *Anal. Chem.* **2005**, *77*, 311−318.
(27) Valaskovic, G. A.; Kelleher, N. L.; Little, D. P.; Aaserud, D. J.; McLafferty, F. W. *Anal. Chem.* **1995**, *67*, 3802−3805.
(28) Chowdhury, S. K.; Chait, B. T. *Anal. Chem.* **1991**, *63*, 1660−1664.
(29) Wu, C.; Siems, W. F.; Asbury, G. R.; Hill, H. H. *Anal. Chem.* **1998**, *70*, 4929−4938.
(30) Clowers, B. H.; Hill, H. H., Jr. *Anal. Chem.* **2005**, *77*, 5877−5885.

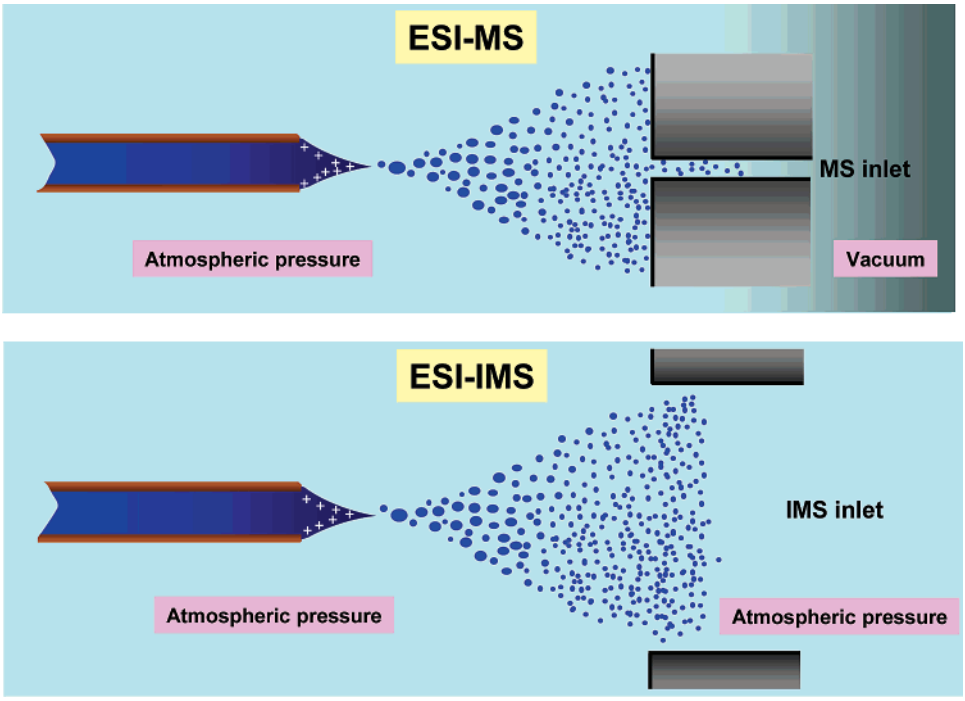

Figure 3. Schematic illustration showing different ion transfer process at the interface of ion source and instrument inlet for ESI-MS and ESI-IMS, respectively.

desolvation of the analyte ions.[22] In analogy, we can deduce that larger cluster solvent ions with longer drift time observed in our experiments were the result of less efficient desolvation at a higher flow rate. The number of clustered solvent ions can be reduced and the solvent peaks shifted to a shorter drift time with a higher drift tube temperature, as reported previously by Wu et al.[29] However, the higher response obtained for the analyte ions at higher flow rates had not been addressed in previous literature.

Ion Transmission in ESI-IMS. Since the flow rate induced opposite effects on ion signals in ESI-IMS and ESI-MS, we speculated that this difference was derived primarily from the different ion transmission processes inherent with these two techniques (Figure 3). In ESI-IMS, ions are created, transferred, and detected in the atmospheric pressure regime throughout. In ESI-MS, on the other hand, ions are formed under atmospheric pressure then transported through various stages of vacuum regions, with gradual reduction in pressure by differential pumping, and finally, detected by MS analyzers at high vacuum. In general, the sensitivity or overall detection efficiency for ESI-MS is determined by two major factors, that is, ionization efficiency and ion transmission efficiency. Nanospray becomes the method of choice due to both its improved ionization efficiency and ion transmission efficiency.[17] It is believed that the small-sized initial droplet emanating from small orifice tip at low flow rate experiences fewer evaporation and fission processes prior to eventual ion formation in the gas phase. Wilm and Mann[14] reported that at 1 μM concentration and sufficiently low flow rate (<40 nL/min), nanospray can produce very small-sized droplets (<200 nm in diameter), which on average contain only one analyte molecule. Thus, ionization efficiency can approach 100% if every analyte molecule is dispersed in a very small charged droplet. With 100% ionization efficiency, the remaining determinant for sensitivity of ESI-MS is ion transmission efficiency. Most ESI-MS instruments employ a very small orifice as the MS inlet using either a small pinhole (~50−200 μm in diameter) or a capillary tube (~0.5-mm i.d.) to achieve the requisite pressure drop between the atmospheric ion source region and the first vacuum stage in MS. However, charged droplets exiting the electrospray Taylor cone are expanding into a plume that is significantly larger than the MS inlet orifice. Consequently, only a small portion of the total ions can be transported into the MS inlet by dynamic gas flow and the potential difference imposed between the spray emitter and the MS inlet (Figure 3). Efforts to increase the size of the MS entrance by using a multicapillary inlet[31] or flared inlet tube[32] have been reported to obtain better sampling efficiency; however, there is an upper limit for the MS inlet size, since a higher pump speed is needed to maintain the low pressure as MS inlet size increases. In this regard, nanoESI is advantageous over conventional ESI in terms of ion transmission efficiency, as well, because closer proximity and in-axis alignment between the nanospray emitter and the MS inlet allows a higher transfer efficiency.[17]

When nanospray is applied to ESI-IMS, the ionization process is similar to that in ESI-MS; however, the ion transfer process is totally different in a couple of aspects. First, without the vacuum restriction, the IMS instrument operated at atmospheric pressure can have the entrance aperture as large as possible to receive 100% of the incoming ion plume (Figure 3). The initial charged droplets or ion plume are drawn into the drift tube by the potential difference applied between the spray tip and the IMS inlet without any gas dynamic disturbance. Second, the Faraday plate detector with the acceptance dimension covering the entire IMS exit aperture allows capturing all arrival ions if no ions are lost during their transmission through the drift space. And finally, ion transfer

(31) Kim, T.; Udseth, H. R.; Smith, R. D. *Anal. Chem.* **2000**, *72*, 5014−5019.
(32) Wu, S.; Zhang, K.; Kaiser, N. K.; Bruce, J. E.; Prior, D. C.; Anderson, G. A. *J. Am. Soc. Mass Spectrom.* **2006**, *17*, 772−779.

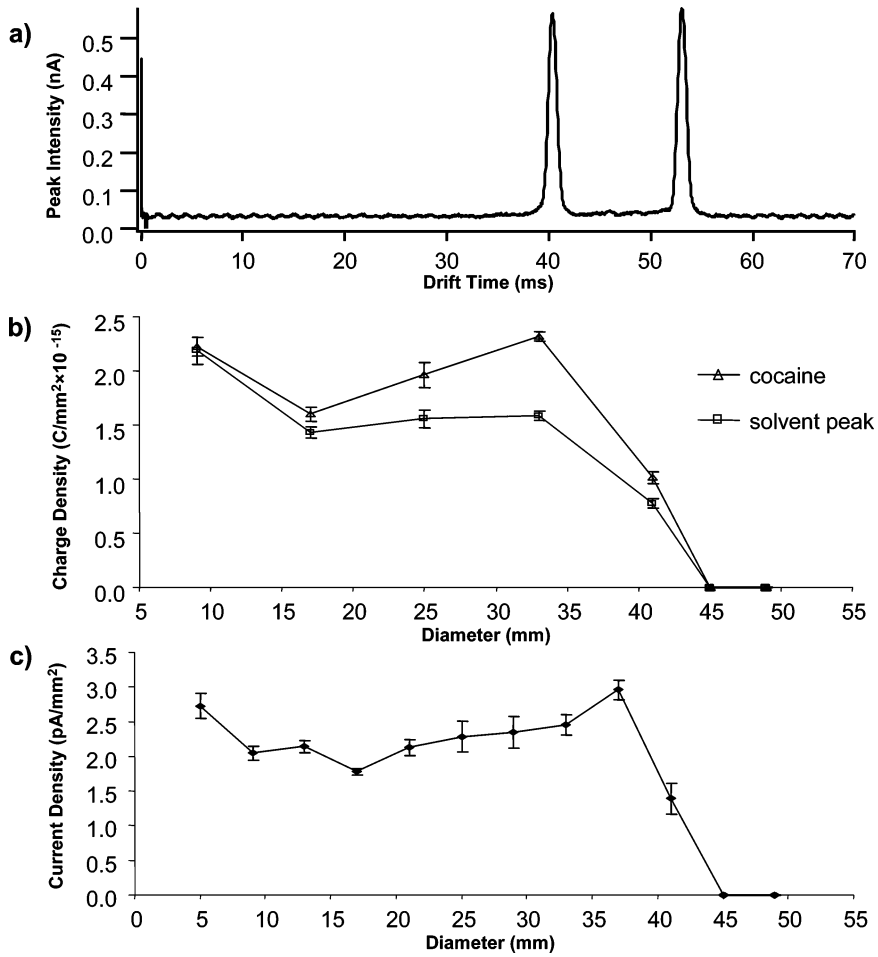

Figure 4. Arrival ion beam charge and current distribution study by a target Faraday detector. (a) ESI-IMS spectrum of 50 μM cocaine. The spectrum was acquired using combined ring 5 and ring 6 in the target detector at room temperature. The peak at drift time of ~40.4 ms is the solvent ion peak, and the peak at drift time of ~53.1 ms is the cocaine ion peak. (b) A plot of charge density (coulomb/mm^2 $\times$ 10^{-15}) as a function of the ring outer diameter (mm) for cocaine ions and solvent ions arrived at the IMS exit. (c) A plot of current density (pA/mm^2) distribution at the IMS terminus versus the ring outer diameter (mm).

is constant, regardless of flow rate variation. However, we know that ion packets injected into the drift tube experience further spatial broadening in the drift region due to thermal diffusion, Coulomb expansion, and electric field inhomogeneity.[29,33] If the width of the ion packets exceeds the inner diameter of the drift tube prior to its arrival at the IMS terminus, then ions are lost, and ion transmission efficiency is reduced. The transmission efficiency through the IMS space alone was assumed to be 100% when Tang et al. demonstrated near-perfect ion transfer through an ion funnel interface for ESI-IMS-MS.[34] Sysoev el al. also concluded that ion loss during transmission through the IMS tube was minimal when they obtained similar signals with and without a modular IMS inserted between the ESI-MS.[35] Gillig et al. simulated ion trajectories inside the drift tube and showed that ions were transferred without any loss through the drift tube when they reported an ion-focusing guide for MALDI-IMS-MS.[36] However, to our knowledge, no direct empirical data has been reported to demonstrate ion transmission is close to 100% in the IMS tube.

To picture the incoming ion beam at the IMS terminus, we designed and incorporated a targetlike segmented Faraday plate detector (Figure 1) to detect arrival ion distribution at the drift tube terminus. Because the nonconductive resin support on which the target detector was mounted is not heat-resistant, the current distribution experiment was performed at room temperature (18 °C) using 50 μM cocaine with the following parameters: 500 mL/min counter flow N_2 drift gas, 2.5 μL/min infusion flow rate, and 15 kV and 11.5 kV applied to the nanospray emitter and the first drift ring, respectively. For IMS spectral acquisition, a combination of 2 adjacent rings was used to ensure good quality for each spectrum, with the exception of rings 11 and 12, where no ion signal was detected. Figure 4a shows an example of an IMS spectrum collected with a combination of rings 5 and 6. Two peaks were detected for each spectrum. The first peak is the solvent peak with a drift time of ~40.4 ms; the second peak is cocaine with a drift time of ~53.1 ms. Note that at room temperature,

(33) Siems, W. F.; Wu, C.; Tarver, E. E.; Hill, H. H., Jr.; Larsen, P. R.; McMinn, D. G. *Anal. Chem.* **1994**, *66*, 4195−4201.
(34) Tang, K.; Shvartsburg, A. A.; Lee, H. N.; Prior, D. C.; Buschbach, M. A.; Li, F.; Tolmachev, A. V.; Anderson, G. A.; Smith, R. D. *Anal. Chem.* **2005**, *77*, 3330−3339.
(35) Sysoev, A.; Adamov, A.; Viidanoja, J.; Ketola, R. A.; Kostiainen, R.; Kotiaho, T. *Rapid Commun. Mass Spectrom.* **2004**, *18*, 3131−3139.
(36) Gillig, K. J.; Ruotolo, B. T.; Stone, E. G.; Russell, D. H. *Int. J. Mass Spectrom.* **2004**, *239*, 43−49.

only one solvent peak was observed, but with a higher drift tube temperature (200 °C), two resolved solvent peaks were observed (Figure 2b). These results were consistent with a previous study by Wu et al., who showed that lower drift gas temperature resulted in fewer and broader solvent peaks due to insufficient desolvation and clustering.[29] The charge density was calculated by dividing the analyte peak area ($Q = It$, where Q is charge in coulomb, I is current in ampere, and t is time in second) by the ring area (mm^2), then plotted against the radius of each ring (Figure 4b). As shown in the Figure, the charge density started to decay when the ring diameter reached over 34 mm, and no ion signal was observed on rings 11 and 12, which covered the diameter of 45 mm and beyond. Approximately 90% of the total charge was found within a 33-mm diameter, suggesting that the arrival ion beam circumference was smaller than the inner diameter (48 mm) of the drift tube. Thus, it can be concluded that no ions were lost to the inner wall of the drift tube, since if any signal was observed in ring 12, one would expect that the ion beam expanded and exceeded the size of drift tube at a certain point during its transmission. To further confirm this conclusion, the total current on each ring was also measured, and current density was calculated and plotted versus its ring radius (Figure 4c). Similarly, most current was found within a 36-mm diameter, and the current rapidly decayed to zero at ring 11.

Electrospray Ionization Efficiency. Higher flow rate tolerance in ESI-IMS than that in ESI-MS was reported previously.[37,38] To explain why flow rate responses behave differently in ESI-IMS and ESI-MS, we need to consider the overall ion detection efficiency (DE%), which ultimately determines the sensitivity of the detection method. Overall ion detection efficiency, defined as total number of ions recorded at the detector (n) divided by the total number of analyte molecules introduced (n'), is dependent on two factors: ionization efficiency (IE%) and ion transmission efficiency (TE%).[39,40] Therefore, we have DE% = $(n/n') \times 100\%$ = IE% × TE%. The bottleneck that limits the ion transmission efficiency due to the small orifice inlet employed in ESI-MS is not a problem for atmospheric pressure ESI-IMS. Ion transfer at the IMS inlet is close to 100% due to the large entrance orifice, and further ion transfer in the drift tube showed minimal loss, as discussed in the target detector study. Importantly, ion transfer in ESI-IMS is constant, regardless of flow rate variations, and ion loss is negligible, as compared to that in ESI-MS. As a consequence, the overall ion detection efficiency in ESI-IMS should be affected by only one variable, ionization efficiency. The overall ion detection efficiency can be calculated from experimental measurements; thus, ionization efficiency can be obtained.

To calculate overall ionization efficiency, first we need to calculate the total number of ions detected by Faraday plate. We know the total charge (Q) in coulombs of all ions is given by

$$Q = It \tag{1}$$

where I is the current in amperes and t is the time in seconds. Q can also be measured from the IMS spectrum, since It = peak area. In addition, according to Coulomb's law,

$$Q = nze \tag{2}$$

where n is the number of ions; z is the charge state of the ion (e.g., $z = 1$ for proton); and e is the charge on one electron, which is 1.602×10^{-19} C. Thus, the total number of ions detected (n) can be calculated by

$$n = \frac{\text{peak area}}{ze} \tag{3}$$

On the other hand, the total number of analyte molecules introduced (n') at the ion source to the drift tube at every gate pulse is equal to

$$n' = cft_gN_{avg} \tag{4}$$

in which c is the molar analyte concentration, f is the flow rate in liters/second, t_g is the gate pulse width in seconds, and N_{avg} is Avogadro's constant (6.0221415×10^{23} mol^{-1}). Thus, the overall detection efficiency (DE%) is given by

$$\text{DE\%} = \frac{\text{peak area}}{zecft_gN_{avg}} \times 100\% \tag{5}$$

TE% is constant in ESI-IMS, and we assume TE% is 100% here, since ion loss is minimal as compared to that in ESI-MS; thus, DE% = IE%. In this regard, atmospheric pressure IMS provides a good tool for characterizing electrospray ionization.

Effects of Analyte Concentration. With the equation for calculating ionization efficiency, we further evaluated the effects of the flow rate on the ionization efficiency by varying the analyte concentration. Cocaine was used as the analyte for this study, with the concentration varying from 10 to 200 μM in a solution of 50% MeOH, 45% H_2O, and 5% HOAc. At each concentration, the IMS spectra were acquired with flow rate varied from 0.05 to 10 μL/min. All the experiments were performed using the same operating parameters: 13.5 kV ESI voltage, 10 kV drift voltage, 8.8 kV gate voltage, 500 mL/min N_2 drift gas flow, and 225 °C oven temperature. Figure 5a shows plots of cocaine peak intensities extracted from IMS spectra as a function of flow rate for different cocaine concentrations. When the concentration was below 50 μM, the response of cocaine steadily increased as the flow rate increased. At concentrations of 100 and 200 μM, the ion signals started to plateau when the flow rate was over 2.5 and 5 μL/min, respectively, indicating that the total number of ions detected at the Faraday detector reached the maximum. These results were consistent with our initial observations described earlier, that is, a higher flow rate produced a higher response. Next, we calculated the ionization efficiency (IE%) using eq 5 and plotted it as a function of the flow rate at different concentrations (Figure 5b). In this case, $z = 1$ since cocaine is detected as a singly charged ion.[38] As predicted from any ESI-MS experience, the ionization efficiency increased when the flow rate decreased. This finding has been known for many years in the field of mass spectrometry, and the theoretical reasoning has also been extensively characterized; nonetheless, this data presented the important empirical

(37) Asbury, G. R.; Hill, H. H., Jr. *Int. J. Ion Mobility Spectrom.* **1999**, *2*, 1−8.
(38) Wu, C.; Siems, W. F.; Hill, H. H., Jr. *Anal. Chem.* **2000**, *72*, 396−403.
(39) Smith, R. D.; Loo, J. A.; Edmonds, C. G.; Barinaga, C. J.; Udseth, H. R. *Anal. Chem.* **1990**, *62*, 882−899.
(40) Cech, N. B.; Enke, C. G. *Mass Spectrom. Rev.* **2001**, *20*, 362−387.

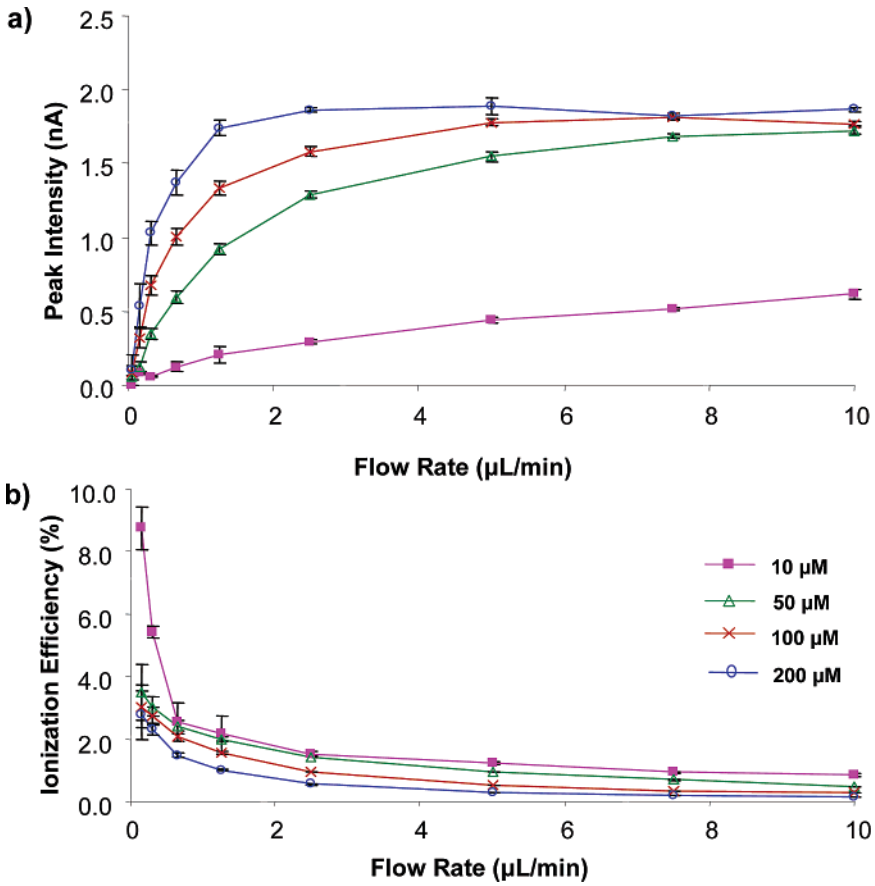

Figure 5. Effects of analyte concentration. (a) Plots of cocaine ion signal intensity as a function of flow rate at four different concentrations. (b) Plots of ionization efficiency versus flow rate for cocaine at four different concentrations. All figure legends are shown in part b.

proof to confirm that ionization efficiency is higher with a lower flow rate. For the first time, the electrospray ionization efficiency can be characterized independently without consideration of the other variable, transmission efficiency, with the use of atmospheric pressure IMS. In addition, Figure 5b also shows the ionization efficiency was lower when the analyte concentration was higher. This is due to the fact that at a higher concentration, the competition among the analyte molecules for available charges on the droplets increases, resulting in fewer analyte molecules ionized.

Regardless of improved ionization efficiency obtained at a lower flow rate and lower concentration, in ESI-IMS, the ion response signal increased with an increasing flow, which is the opposite of the trend observed in ESI-MS. We know that ion signal intensity is directly related to the total number of ions captured (n) by the detector, which is proportional to both DE% and the total number of analyte molecules injected (n') at the ion source.

$$n = n'\mathrm{DE}\% = cft_g N_{\mathrm{avg}}\mathrm{DE}\% \qquad (6)$$

Although the ionization efficiency decreases, the absolute amount of analyte (n') introduced increases at a higher flow rate and dominates eq 6, thus contributing to a higher signal response. When the flow rate further increases and ionization efficiency further decreases and becomes the dominating factor, the ion response will plateau and eventually decrease. We did not carry out any experiments with flow rate over 10 μL/min due to the backpressure restriction from the spray emitter; however, the observation that the signal response decreased at a substantially high flow rate with a 50-μm-i.d. emitter was reported previously.[37]

Effects of Solvent Composition. A composition ratio of 1:1, water and organic solvent (methanol or acetonitrile), with 0.1−5% ion paring agent, such as acetic acid, formic acid, or trifluoroacetic acid, is often used as an electrospray solution for most analytes. Organic modifier has a lower surface tension than water, which helps disperse charged droplets into smaller droplets and, thus, promote ionization efficiency. In addition, organic solvent helps improve desolvation due to its higher volatility. To test the influence of solvent composition on ionization efficiency, 50 μM cocaine solutions prepared in five different solvent buffers with varying MeOH composition (0, 25, 50, 75, and 95%) and 5% HOAc in water were used. The following conditions were applied for this set of experiments: 13 kV ESI, 10 kV drift voltage, 8.8 kV gate voltage, 500 mL/min N_2 drift gas, and 225 °C oven temperature. The cocaine peak intensity was plotted against the flow rate, and the results are shown in Figure 6a. The general trend of an increasing response with increasing flow rate was observed in this case, as well. Moreover, the ion signals generally appeared to be higher with a higher percentage of MeOH, with the exception of 95% MeOH. We further calculated ionization efficiency for each data point in Figure 6a and plotted it versus the flow rate (Figure 6b). Once again, we observed the general trend that a lower flow rate had a better ionization efficiency and the inclusion of organic solvent helped improve ionization efficiency. However, in the case

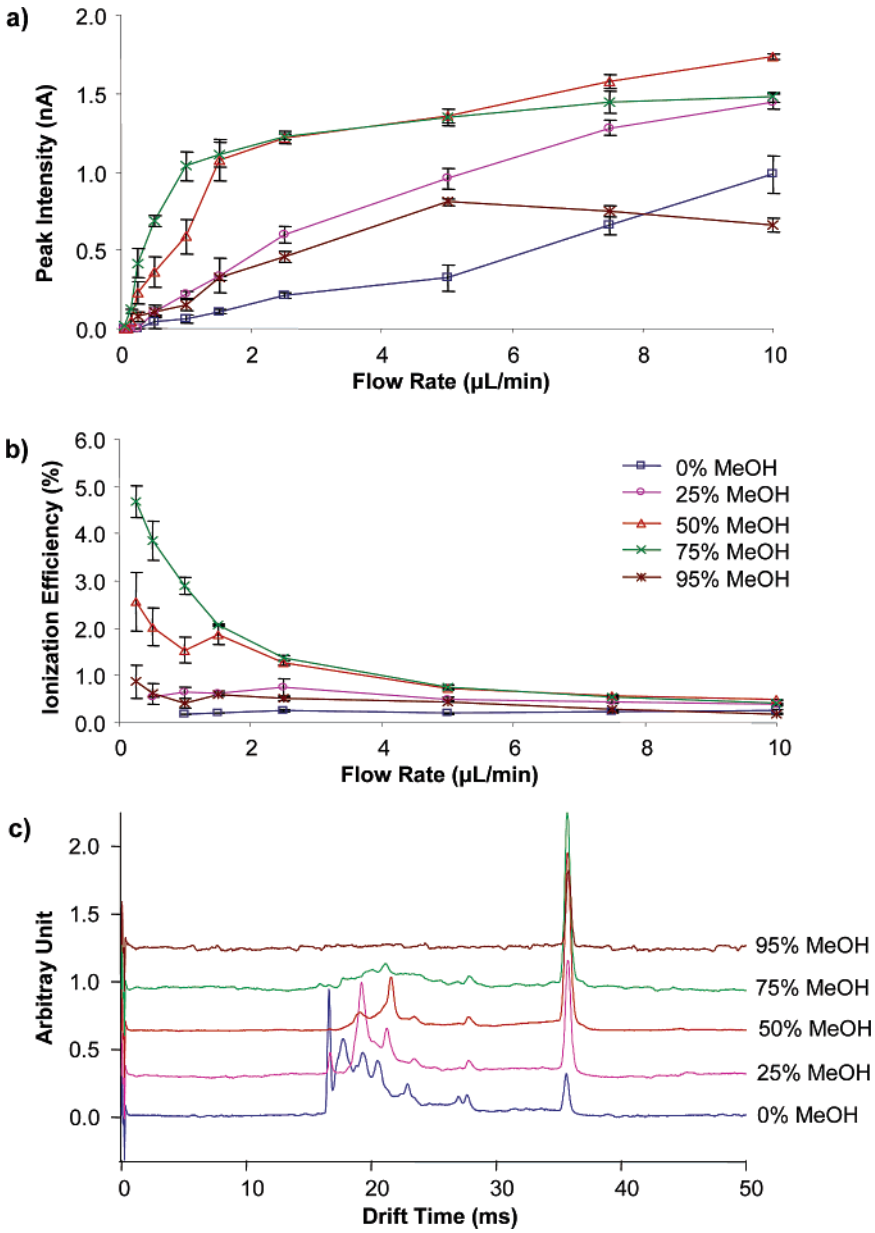

Figure 6. Effects of solvent composition. (a) Plots of cocaine ion signal intensity as a function of flow rate for five different solvents, with MeOH percent varying from 0 to 95%. (b) Plots of cocaine ionization efficiency versus flow rate for five different solvents. Both a and b figure legends are shown in part b. (c) ESI-IMS spectra of 50 μM cocaine solution in five different solvents.

of 95% MeOH and 5% HOAc with no H_2O, the ion signal and ionization efficiency started to reduce. When comparing the individual IMS spectra with the different flow rates and different MeOH compositions, two basic tendencies appeared obvious. First, the solvent cluster peaks shifted to a higher drift time and decreased in peak intensity with a higher flow rate (data not shown in this case, but similar results are shown in Figure 2b). This indicated that the solvent cluster was growing bigger, leading to slower mobility, and was ionized less efficiently as a result of the increased flow rate. Second, with more MeOH and less H_2O included in the solvent, less and weaker solvent cluster peaks were observed (Figure 6c). No solvent peaks were observed in the case of the 95% MeOH throughout all of the flow rate variations. All of these observations indicated that a certain amount of H_2O is necessary for efficient electrospray ionization. Water tends to produce clusters more easily than MeOH, due probably to the strong hydrogen bonding of water molecules. This clustering equilibrium between H_2O and analyte molecules in the gas phase and continuous consumption of analyte$-H_2O$ clusters as a result of complete desolvation of analyte will push the chain reactions forward to create more "naked" analyte ions. This could explain why we observed a signal decrease when no H_2O was included in the case of 95% MeOH. Thus, taken together, we think that although the inclusion of a certain amount of MeOH is necessary to help better ionization because of its lower surface tension and higher volatility, a certain amount of H_2O should also be included to improve ionization.

CONCLUSIONS

This report has presented the first comprehensive study of the effects of flow rate ranging from nanoliter per minute to microliter per minute for ESI-IMS. The general tendencies to

obtain higher signals from higher flow rates appeared to be surprising at first glance. However, after thorough and careful analysis, these opposite effects were attributed to the different ion transmission mechanisms that exist in ESI-IMS and ESI-MS. Our data showed that the general recognition of improved ionization efficiency at reduced flow rate for ESI-MS still held true in the case of ESI-IMS, despite the ion signal loss's being observed. On the basis of our ionization efficiency analysis, now we are able to understand why no substantial sensitivity improvement was observed for nanoESI-IMS (use of >5 mM analyte concentration),[23] as compared to nanoESI-MS, which shows a signal enhancement of at least 2 orders of magnitude over conventional ESI-MS.[14] Thus, it seems necessary to further improve ionization efficiency for IMS to improve overall detection sensitivity. However, the inherent limitation of IMS is attributed to its low duty cycle (<1%). Improving the duty cycle is the fundamental solution for improving the sensitivity of IMS, as demonstrated recently by using the Hadamard transform[41] modes of operation, which resulted in significant signal gains. On the other hand, it is believed that the limiting factor for the sensitivity of ESI-MS is the ion transfer process from the atmospheric region to the low-vacuum region in MS.[42] However, the efficiency of the ion transfer process for ESI-MS is still unclear because the efficiency of the ionization process is also unclear. On the basis of our measurements of ionization efficiency, the ion transfer efficiency for ESI-MS can be estimated. The ionization efficiency was assumed to be near 100% for spraying 1 μM analyte at 20 nL/min (one molecule per charged droplet),[14] but at 2 μL/min, the ionization efficiency is estimated to be ~2% according to our data. Thus, if assuming the signal gain is ~100-fold with the use of nanospray, as opposed to conventional spray, the ion transfer efficiency is ~200 times higher in nanospray than that in conventional spray. The overall ion transfer efficiency for conventional spray was reported to be ~0.001% (at the detector).[42] Thus, for nanospray, the overall ion transfer efficiency is ~0.2%. Therefore, there is still room for improving the ion transfer efficiency, which will ultimately contribute to the overall sensitivity improvement for ESI-MS.

Our study also presented a new perspective of IMS that has not been employed previously. The unique constant ion transmission property and atmospheric ion detection property allow IMS to characterize the ionization process for different analytes at various flow rates, concentrations, and solvent compositions, as demonstrated in this study. However, IMS certainly can be used to characterize and evaluate any type of atmospheric pressure ion sources in addition to ESI, such as atmospheric pressure MALDI,[43] desorption electrospray ionization,[44] or any new modifications made to the ion sources, for example, a multisprayer emitter.[45] We believe the knowledge gained from IMS ionization characterization could further provide insight for new method development and improvement and eventually enhance the sensitivity for both IMS and MS techniques.

ACKNOWLEDGMENT

This research was supported by grants from the National Institutes of Health, Grant No. R21 DK070274; the Office of Science (BER), U.S. Department of Energy, Grant No. DE-FG02-04.ER63924; and National Science Foundation, Grant No. DBI-0352451.

AC0613380

(41) Clowers, B. H.; Siems, W. F.; Hill, H. H.; Massick, S. M. *Anal. Chem.* **2006**, *78*, 44−51.
(42) Zook, D. R.; Bruins, A. P. *Int. J. Mass Spectrom. Ion Processes* **1997**, *162*, 129−147.
(43) Laiko, V. V.; Moyer, S. C.; Cotter, R. J. *Anal. Chem.* **2000**, *72*, 5239−5243.
(44) Takats, Z.; Wiseman, J. M.; Gologan, B.; Cooks, R. G. *Science* **2004**, *306*, 471−473.
(45) Tang, K.; Lin, Y.; Matson, D. W.; Kim, T.; Smith, R. D. *Anal. Chem.* **2001**, *73*, 1658−1663.